Korean J. Chem. Eng., 34(1), 110-117 (2017)
DOI: 10.1007/s11814-016-0220-5

pISSN: 0256-1115
eISSN: 1975-7220

Synthesis and characteristics of lignin-derived solid acid catalysts for microcrystalline cellulose hydrolysis

Jundong Zhu, Linhuo Gan†, Baoxia Li, and Xin Yang

College of Chemical Engineering, Huaqiao University, Xiamen 361021, China
(*Received 9 March 2016 • accepted 1 August 2016*)

Abstract−Three kinds of solid acid catalysts were prepared from alkali lignin in the waste liquor of pulping using carbonation-sulfonation method with different pretreatment. The lignin-derived solid acids (LDSAs) were characterized by FESEM, XRD, FTIR, TGA, BET and acid-base titration, respectively. A comparison study on the catalytic performance of LDSA prepared by different pretreatment method before carbonation in the hydrolysis of microcrystalline cellulose (MCC) was carried out. Results showed that the LDSA prepared by chemical activation with phosphoric acid (LPC-SO_3H) exhibited superior catalytic activity due to its higher densities of -COOH group (1.68 mmol/g) as binding site and -SO_3H group (0.88 mmol/g) as catalytic site as well as its larger specific surface area (488.4 m^2/g) than those of the other two LDSAs. A total reducing sugar yield of 50.8% in MCC hydrolysis was obtained under the reaction conditions of temperature of 180 °C, time of 3 h, MCC concentration of 6 mg/mL and mass ratio of catalyst to MCC of 3.3 (w/w). Additionally, the value activation energy for hydrolysis of MCC to reducing sugars using LPC-SO_3H was 83.31 kJ/mol, which was smaller than that using sulfuric acid.

Keywords: Lignin, Carbon-based Solid Acid, Catalyst, Cellulose Hydrolysis

INTRODUCTION

Heterogeneous solid acid catalysts, which are separable and reusable, have many advantages over homogeneous liquid acid catalyst from the viewpoint of green chemistry and industrialization [1-3]. Generally, solid acids with good catalytic activities possess both catalytic sites and adsorption sites as well as larger specific surface area [4,5]. Many kinds of solid acid catalysts, such as zeolites [6], metal oxides [7], heteropolyacid [8], nafion [9] and sulfonated resins [10], have been used widely in cellulose hydrolysis. However, their catalytic performance is still relatively low due to few effective sites and poor catalytic stability [11,12]. As a result, the development of a novel low-cost solid acid catalyst with efficient catalytic activity is necessary and significant.

With the increasing scarcity of oil resource and awareness of environmental protection, the synthesis of biomass-based material has been widely recognized [13,14]. Among them, various carbonaceous solid acid catalysts for the hydrolysis of cellulose to glucose have been widely reported [15,16]. Hara et al. used carbohydrates to synthesize carbon-based solid acid catalysts through incomplete carbonation followed by sulfonation, and the catalysts showed good activities in the hydrolysis of cellulose [17]. However, due to the small specific surface area of carbonaceous solid acid catalyst derived from carbohydrates, cellulose is less accessible to the active sites on catalyst surface [18]. Guo et al. designed and synthesized a glucose-based solid acid catalyst using hydrothermal carbonization followed by sulfonation. The carbonaceous catalyst with phenolic -OH, -COOH, and -SO_3H groups exhibited good catalytic activity for the hydrolysis of cellulose, and a total reducing sugar (TRS) yield reached up to 72.7% in ionic liquid ([BMIM]Cl) system at 110 °C for 4 h [19]. Unfortunately, due to the high cost and low stability of ionic liquids in the present technologies, their mandatory requirements such as quantitative recovery and reuse hinder their industrial applications in the hydrolysis of cellulose. Generally, water is considered as the most common solvent system from an economic and environmental point of view; it is very meaningful to study the hydrolysis of cellulose with high efficiency in aqueous solution [20,21].

Owing to the increasing demands of value-added products from lignocellulose, the high-value utilization of lignin has been widely concerned [22,23]. Lignin is an abundant renewable biomass resource, with the richest aromatic structure among natural organic materials. In China, large amounts of alkali lignin recovery from pulping waste are regarded as waste landfill or burned directly. Only a small part has been used for the preparations of carbon fiber [24], water-reducing agent [25] and dispersing agents [26], etc. To broaden the high-value utilization of lignin, Hu et al. prepared a magnetic lignin-derived solid acid catalyst by using the enzymatic hydrolysis lignin residue, which exhibited good activity in the hydrolysis of cellulose in the presence of ionic liquid [27]. Hu et al. synthesized a lignin-derived solid acid catalyst through direct sulfonation of activated carbon fibers from lignin; a glucose yield of 29.9% in the hydrolysis of rice straw cellulose was achieved at 150 °C and 5 atm [28]. Nevertheless, it is far from enough to activate the high value-added utilizations of technical lignin; many more potential applications should be encouraged and exploited.

In this study, we synthesized a novel lignin-derived solid acid (LDSA) from alkali lignin in black liquor of soda pulping by carbon-

†To whom correspondence should be addressed.
E-mail: lhgan401@126.com

ation-sulfonation method. To improve the catalytic activity of catalyst, a comparison study on the catalytic performance of LDSA prepared by different pretreatment method before carbonation in the hydrolysis of microcrystalline cellulose (MCC) was made for the first time. Three solid acids synthesized by different preparation methods were characterized by means of FESEM, XRD, FTIR, TGA, BET and acid-base titration. We believe that these research results will contribute to a better understanding of structure-performance relationship of LDSA in hydrolysis of cellulose as well as the high-value utilization of lignin separated from natural lignocellulose.

EXPERIMENTAL

1. Materials

Masson pine alkali lignin (MAL), which was separated and purified from masson pine pulping black liquor using acidic treatment, was supplied by Nanping Paper-making Co. Ltd. (Fujian, China), MCC (25 μm), glucose, 3, 5-Dinitrosalicylic acid (DNS) were purchased from Aladdin Chemistry Co. Ltd. (Shanghai, China). Nitrogen (purity 99.999%) was purchased from Chenggong Gas Co. Ltd. (Xiamen, China). H_2SO_4 (purity 98%) and H_3PO_4 (purity 85%) were obtained from Xilong Chemical Co. Ltd. (guangzhou, China). NaOH, NaCl, $NaHCO_3$, $BaCl_2$, and other reagents were AR grade and purchased from Kezhan Chemical Glass Instrument Co. Ltd. (Xiamen, China).

2. Purification of Carbonaceous Precursor

MAL was dissolved in 10% NaOH aqueous to remove impurities. Then MAL was precipitated by adding H_2SO_4 till solution pH was nearly 3. The solution was then heated 80 °C and stirred at 200 rpm for 3 h. The precipitate was washed using deionized water for several times until solution pH reached neutral, and was dried overnight at 60 °C, Next, the dried MAL was ground to 100 mesh as the carbonaceous precursor for the preparation of catalyst.

3. Preparation of Lignin-derived Solid Acid Catalysts

10 g MAL was impregnated with 40% H_3PO_4 aqueous solution by phosphoric acid-to-lignin mass ratio of 1.5, and heated at 80 °C for 6 h. Next, the mixture was carbonized at 450 °C for 90 min at 75 mL/min nitrogen flow in a tube furnace. Then, the carbonized mixture was washed several times with hot deionized water until solution pH approximated neutral, and was dried in oven at 105 °C for 12 h to obtain the lignin-derived carbonaceous material (LDCM). The prepared LDCM was added into the concentrated sulfuric acid (m/v, 1 g/20 mL) under nitrogen atmosphere at 180 °C for 12 h. After cooling at room temperature, the black slurry was washed with hot water (>80 °C) until no detection of SO_4^{2-} in the filtrate, then the sulfonated product was dried at 60 °C in oven for 8 h to obtain the first LDSA sample, and the carrier and catalyst were labeled as LPC and LPC-SO_3H, respectively. The second LDSA sample was prepared by the direct carbonization of MAL first and followed by the sulfonation, and the corresponding carrier and catalyst were labeled as LC and LC-SO_3H, respectively. Finally, 10 g MAL was added into 100 mL, 35% H_2SO_4 and the mixture was hydrothermally treatment at 140 °C for 2 h in a Teflon-lined autoclave reactor. This mixture was carbonized in nitrogen atmosphere and sulfonated in concentrated sulfuric acid to obtain the third LDSA sample. The corresponding carrier and catalyst were labeled as SLC and SLC-SO_3H, respectively. All samples of catalyst prepared are of size 0.075 mm and below.

4. Catalysts Characterization

Ultimate analysis of MAL involved a EuroEA3000 analyzer. Proximate analysis of MAL was by measuring volatile matter (900 °C in nitrogen atmosphere) and ash (incineration at 815 °C in air) according to Chinese Standard GB/T212-2001. The MAL, MAL activated by phosphorylation (MALP), and MAL pretreated hydrothermally in H_2SO_4 (MALS) deposition measurement were carried out on Shimadzu DTG-60H thermogravimetric analyzer in a temperature range of 30-800 °C under N_2 at a constant heating rate of 10 °C/ min. Fourier transform infrared spectroscopy (FTIR) spectra of LDSA samples were recorded on a Nicolet iS50 FTIR spectrometer for KBr pellets in a range of 4,000 to 400 cm^{-1} and 32 scans per sample. Nitrogen adsorption-desorption isotherms of the samples were determined on Quantachrome Autosorb-IQ gas adsorption analyzer at −196 °C. The specific surface area and pore size distribution of samples were calculated according to the BET method. The morphologies of carriers and LDSA catalysts were observed by Hitachi SU8000 field emission scanning electron microscopy operated (FESEM) operated at 3 kV. X-ray diffraction pattern were recorded on Rigaku/SmartLa X-Ray diffractometer (XRD) with Cu Kα radiation source at 40 kV and 30 mA from 10° to 80° (2θ) at a scanning speed of 4°/min.

5. Hydrolysis of MCC and Determination of TRS Yield and MCC Conversion

The hydrolysis reaction of MCC was in a 25 mL Teflon-lined stainless steel reactor. 0.025 g of MCC, 0.1 g of catalyst and deionized water (5 mL) were added into the reactor. The mixture was shaken intensively (200 rpm) on a shaking table for 5 min. Subsequently, the reaction was heated at desired reaction temperature for certain time. After reaction, the reactor was cooled to the room temperature immediately. The suspension was then filtered using 0.22 μm filter membrane, and the TRS yield in filtrate was determined using DNS colorimetry as described in literature [28]. The yield of TRS and MCC conversion were calculated based on the Eqs. (1) and (2), respectively.

$$\text{TRS yield}\ (\%) = \frac{C \times V}{30} \times 100 \tag{1}$$

$$\text{Conversion}\ (\%) = \frac{30 - m}{30} \times 100 \tag{2}$$

where C is the total reducing sugar concentration (mg/mL) determined by DNS colorimetric titration and V is the volume of hydrolysate (mL); m is the remaining amount of cellulose after hydrolysis (mg).

6. Acid-base Titration of Functional Groups over LDSAs

The loading amounts (mmol/g) of -SO_3H, -COOH, phenolic -OH groups and total acids in catalyst were estimated using the acid-base back titration modified from literature [29]. First, 0.1 g of catalyst was added into 20 mL, 2 mol/L NaCl aqueous solution, then the mixture was evaporated at room temperature for 24 h and centrifuged. The filtrate was titrated with 6 mmol/L NaOH aqueous solution using phenolphthalein as indicator. The loading amount

Table 1. Ultimate and proximate analyses of purified MAL

Ultimate analysis (wt%, dry basis)				Proximate analysis (wt%)			
C	H	N	O	Moisture	Fixed carbon	Volatile matter	Ash
60.68	5.79	0.12	33.51	8.78	36.36	53.46	1.40

of -SO_3H group could be obtained. Second, 0.05 g of catalyst was put into 20 mL, 0.01 mol/L NaOH aqueous solution; the mixture was evaporated at room temperature for 24 h and was centrifuged. The filtrate was titrated with 0.1 mol/L HCl aqueous solution using phenolphthalein as indicator. Thus, the loading amount of total acids in catalyst was obtained. Finally, 0.05 g of catalyst was put into 20 mL, 0.01 mol/L $NaHCO_3$ aqueous solution; the mixture was evaporated at room temperature for 24 h and then centrifuged. The filtrate was titrated with 0.1 mol/L HCl aqueous solution using phenolphthalein as indicator. Then the loading amounts of -COOH group and phenolic -OH group could also be determined.

RESULTS AND DISCUSSION

1. Characterizations

1-1. Ultimate and Proximate Analyses

Table 1 shows the ultimate and proximate analyses of purified MAL. As listed, the carbon content and ash content of MAL are 60.68% and 1.4%, respectively. It is shown that MAL is an appropriate precursor for preparing carbonaceous material. As is known, alkali lignin is a recyclable by-product from the waste liquor of pulping. Thus, from an economic and environmental point of view, MAL should be considered as a valuable carbon source for preparing carbon-based solid acid.

1-2. TGA Analyses

The TGA curves of MAL, MALP and MALS are illustrated in Fig. 1. As shown, the weight loss of MAL (around 8%) mainly caused by the evaporation of adsorbed water is higher than those of MALP and MALS (approximately 5%) in the temperature range from 30 °C to 150 °C. The 67.5% weight loss of MAL occurring mainly at 150-600 °C is due to the loss of volatiles and tar. Meanwhile, the weight loss rate of MALP (24.85%) is lower than that of MAL within 250-600 °C, which may be attributed to the occurrence of carbonization and aromatic structure among MALP by activation with H_3PO_4 [30,31]. The weight loss of MALS is nearly 35% during 300-600 °C, which is probably due to the decrease in degradation of lignin structure as well as its polymerization through the hydrothermal pretreatment in sulfuric acid [32]. Results show that the pretreatment for MAL has a significant effect on its pyrolysis characteristics, and 450 °C is proper for the carbonization process selected.

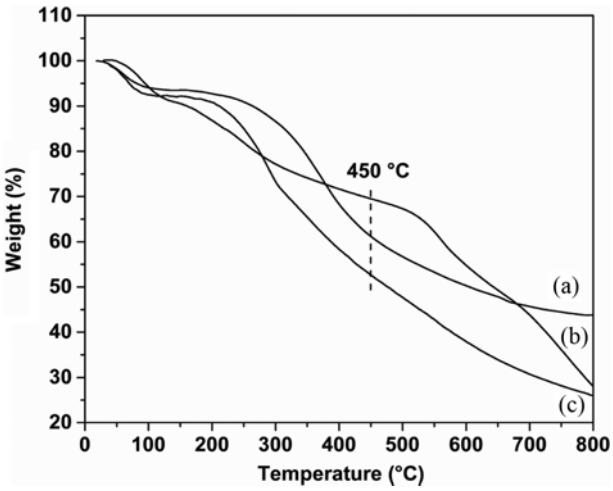

Fig. 1. TGA curves of MALS (a), MALP (b) and MAL (c).

1-3. XRD Analyses

Fig. 2 shows the XRD patterns for LC-SO_3H, SLC-SO_3H and LPC-SO_3H. The patterns exhibit two weak and broad diffraction peaks at 2θ=15-30° and 2θ=35-50°, which are attributed to the amorphous aromatic carbon sheets oriented in random fashion [17]. The lower and wider these peaks are, the higher is the degree of amorphous aromatic carbon sheets. Furthermore, compared with the diffraction patterns of LC-SO_3H and SLC-SO_3H, the diffraction peak of LPC-SO_3H became sharper. The result confirms an increase in crystallinity and the introduction of -SO_3H group into LPC-SO_3H structure, which can be beneficial to the enhancement of catalytic activity in MCC hydrolysis.

1-4. FESEM Analyses

The FESEM images of LDCM and their corresponding LDSAs are presented in Fig. 3. It is clear that the surface morphology of LDCMs is different from that of the corresponding LDSAs. The surface of LDSA becomes relatively rough and turns into a kind of layer structure covered by many irregular particles, which is probably due to the release of water and volatile matters during carbon-

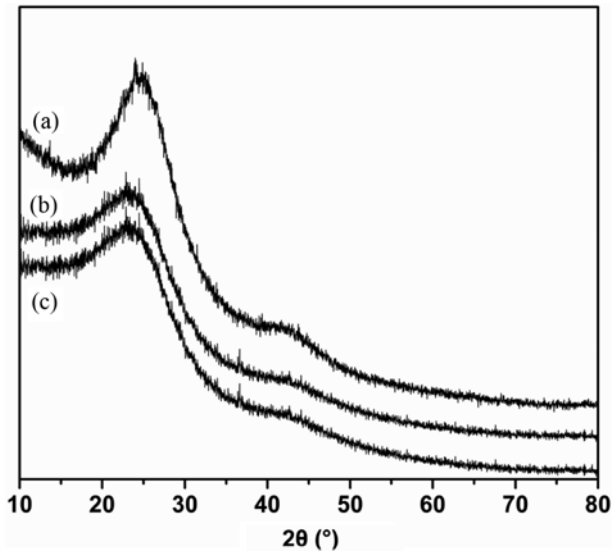

Fig. 2. The powder XRD patterns of LPC-SO_3H (a), SLC-SO_3H (b) and LC-SO_3H (c).

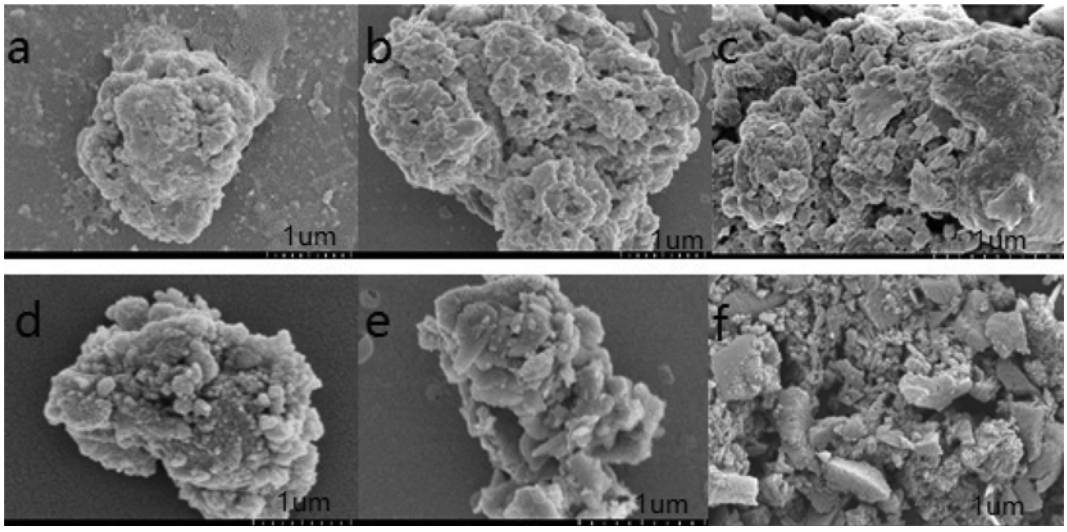

Fig. 3. FESEM images of LDCMs: LC (a), SLC (b), LPC (c) and the corresponding LDSAs: LC-SO_3H (d), SLC-SO_3H (e) and LPC-SO_3H (f).

Table 2. BET measurements for MAL, LPC and LDSAs

Sample	S_{BET} (m^2/g)	V_t (cm^3/g)	D_p (nm)
MAL	56.8	0.054	--
LC-SO_3H	73.7	0.066	--
SLC-SO_3H	66.9	0.062	--
LPC	1454.7	0.790	3.42
LPC-SO_3H	488.4	0.281	2.30

ization and sulfonation processes.

1-5. BET Analyses

The structural characteristics of MAL, LPC and three catalysts are further analyzed by BET, and the results are listed in Table 2. MAL, LC-SO_3H and SLC-SO_3H are carbonaceous materials without pore structure, but LPC and LPC-SO_3H are typical porous materials. It is suggested that phosphorylation pretreatment promotes the formation of highly porous structure in LPC. However, after sulfonation, the specific surface area and pore volume decrease from 1454.7 to 488.4 m^2/g and 0.790 to 0.281 cm^3/g, respectively. These may be due to the structural shrinkage by the treatment of strong acid [23].

1-6. FTIR

The FTIR spectra of LDSA samples prepared by different methods are depicted in Fig. 4. The broad absorption band at around 3,400 cm^{-1} is attributed to O-H stretching vibration. The peaks at 1,165 cm^{-1} and 1,030 cm^{-1} originate from the O=S=O symmetric and asymmetric stretching vibrations, highlighting the successful introduction of -SO_3H groups into LDCM by sulfonation and the formation of C-O-SO_3H structure [17,29]. The band at 1,701 cm^{-1} is assigned to C=O bending vibration [33], indicating the existence of functional -COOH groups on the LDSA surface. Thus, these catalysts prepared by different pretreatment methods had the same acidic functional groups.

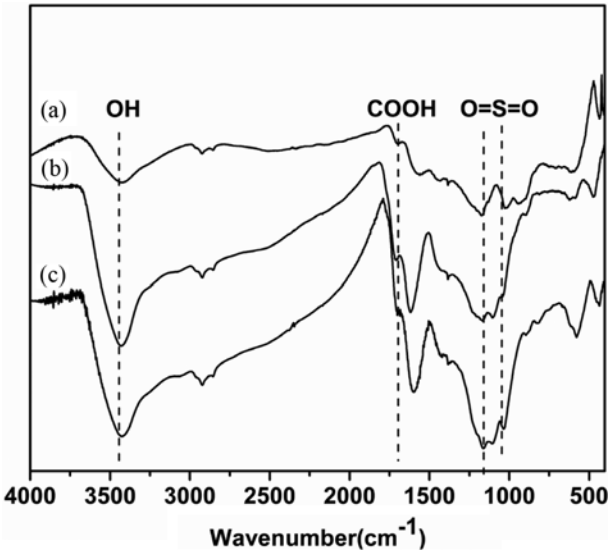

Fig. 4. FTIR spectra of LPC-SO_3H (a), LC-SO_3H (b), SLC-SO_3H (c).

2. Catalytic Activity

As shown in Table 3, all three LDSAs show effective catalytic activities for MCC hydrolysis to TRS. It is surprising that LPC-SO_3H exhibits superior catalytic activity compared to LC-SO_3H and SLC-SO_3H, and a TRS yield of 50.8% is achieved at 180 °C

Table 3. Measurement results of densities of acidic groups and catalytic performances of three LDSAs

Catalyst	Total acid (mmol/g)	-SO_3H (mmol/g)	Phenolic -OH (mmol/g)	-COOH (mmol/g)	TRS yield/%
LPC-SO_3H	3.52	0.88	0.96	1.68	50.8
SLC-SO_3H	2.40	0.85	0.59	0.96	41.1
LC-SO_3H	1.46	0.76	0.58	0.12	20.4

and 3 h. According to the analysis on the concentrations of acidic groups, it seems to have a certain relationship between concentrations of surface acidic groups and catalytic activity of catalyst.

Measurement results of densities of acidic groups in three LDSAs are shown in Table 3. The density of -SO_3H group is about 0.8 mmol/g. However, the density of -COOH group exhibits an obvious difference. The carboxylic density of LPC-SO_3H is the highest (1.68 mmol/g), and the carboxylic density of LC-SO_3H is the lowest (0.12 mmol/g). These results imply that -COOH group is probably more accessible to hydrolyze cellulose into water-soluble β-1, 4 glucan and glucose, and mainly affect the catalytic activity [34-36].

LPC-SO_3H contains abundant acidic functional groups and pore structure; the -COOH groups with high density can form strong hydrogen bonds with the hydroxyl groups of MCC, and can also adsorb or attach to β-1,4-glycosidic bonds on the cellulose chains in water; then -SO_3H groups can hydrolyzed MCC effectively [34,35], as illustrated in Fig. 5. Thus, the MCC molecules can diffuse and expose to the acid sites on the surface of catalyst more accessible, and are hydrolyzed into oligosaccharides and glucose. However, both LC-SO_3H and SLC-SO_3H are inaccessible to β-1, 4-glycosidic bonds on cellulose chains. It is suggested that the adsorption capability of carboxyl groups can effectively will solve the problem of proton diffusion in homogeneous catalysis, which is conducive to promoting efficient hydrolysis of cellulose.

2-1. Effects of Reaction Temperature and Time on the Hydrolysis of MCC

The effects of hydrolysis temperature and time on the conversion of MCC and the yield of TRS during the hydrolysis were investigated, respectively. As shown in Fig. 5(a), the conversion of MCC increases with the reaction temperature and time. At 180 °C, MCC conversion rate increases to 69.7%. Owing to the strong hydrogen bonding interactions, MCC cannot be decomposed completely. Therefore, as the reaction time is further prolonged, MCC conversion rate gradually becomes stable. The influence of reaction temperature and time on MCC hydrolysis to TRS catalyzed by LPC-SO_3H is shown in Fig. 5(b). The results show that the yield of TRS increases first and then decreases as the reaction time is prolonged at 170 °C, 180 °C and 190 °C, respectively. This can probably be explained by the extremely unstable glucose as intermediate product of reaction system, which would be easily further hydrolyzed to HMF and levulic acid at higher temperature (≥160 °C), and is not beneficial to the accumulation of TRS [37,38]. Moreover, the variation of TRS yield is significant with the increasing temperature. The higher the reaction temperature is, the shorter is the reaction time to achieve the maximum yield of TRS. Therefore, considering the reaction temperature and time as well as the TRS yield, the optimal hydrolysis temperature and time are 180 °C and 3 h, respectively.

2-2. Effect of the MCC Concentration and Mass Ratio of Catalyst to MCC on the Hydrolysis of MCC

Hydrolysis was conducted at various MCC concentration from 5 mg/mL to 10 mg/mL and the results are shown in Fig. 6(a). The effect of MCC concentration on the yield of TRS is obvious. A rel-

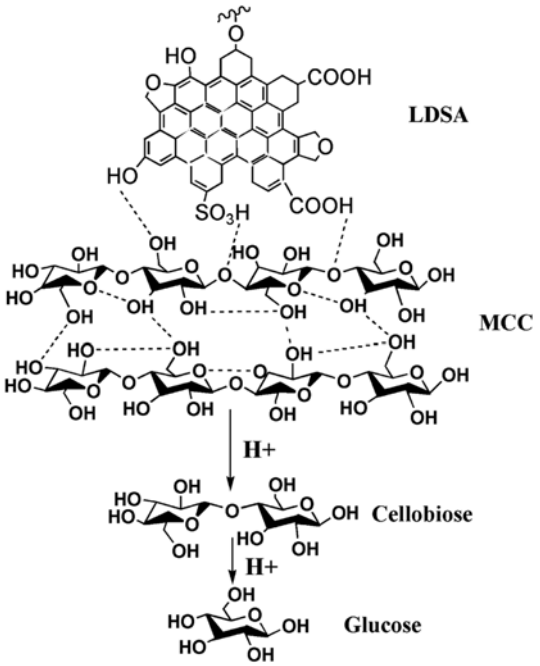

Fig. 5. Plausible mechanism for the hydrolysis of MCC over LDSA.

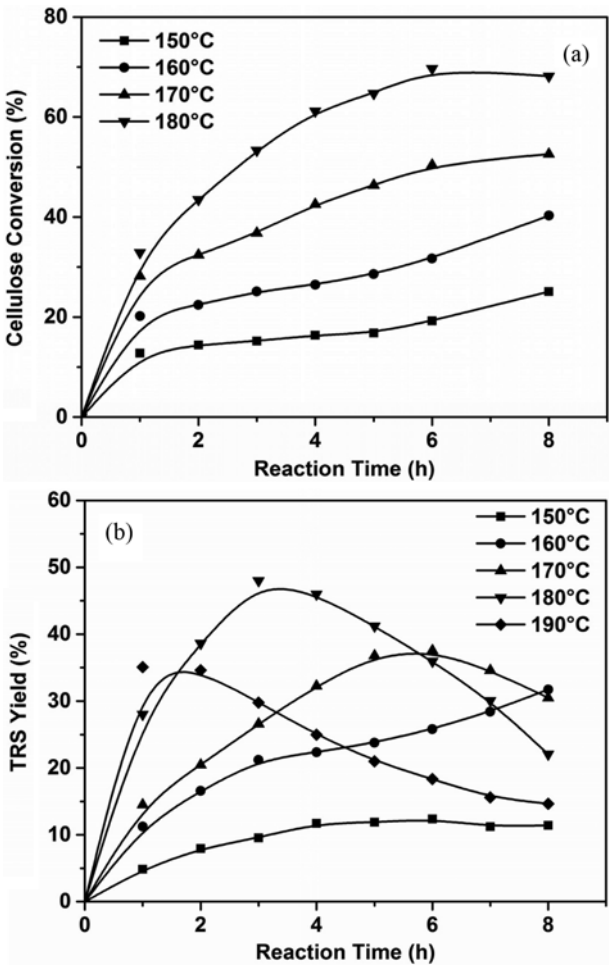

Fig. 6. Effects of reaction temperature and time on the conversion of MCC (a) and TRS yield (b) (0.025 g of MCC, 0.1 g of catalyst, 5 mL of water).

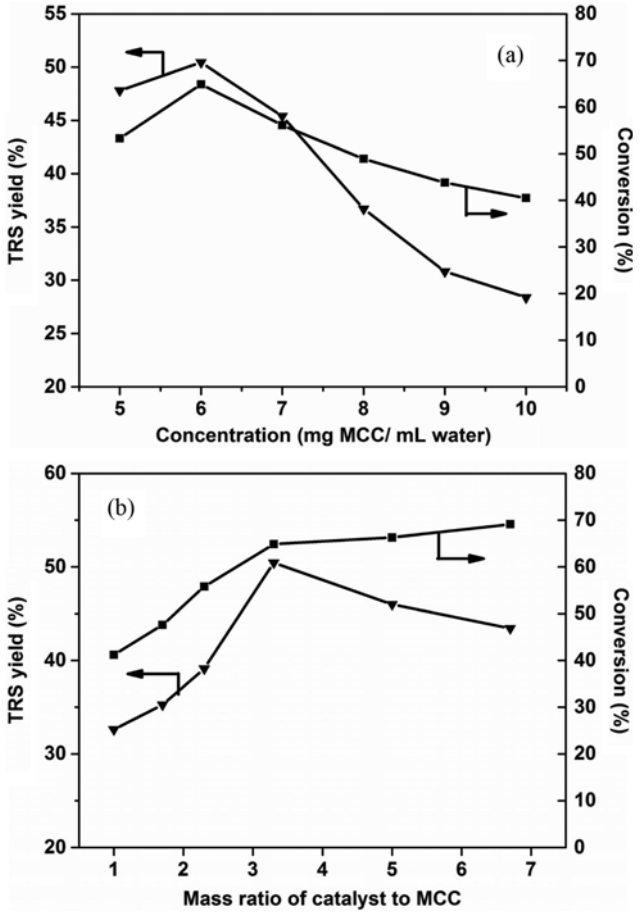

Fig. 7. Effect of MCC concentration (a) and mass ratio of catalyst to MCC (b) on the conversion of MCC and TRS yield (180 °C of reaction temperature, 3 h of time, 5 mL of water).

atively high TRS yield of 50.8% was obtained when MCC concentration was 6 mg/mL. Furthermore, the correlation between TRS yield and catalyst amount is depicted in Fig. 6(b). TRS yield increased from 29.0% to 50.8% as mass ratio increased from 1 to 3.3

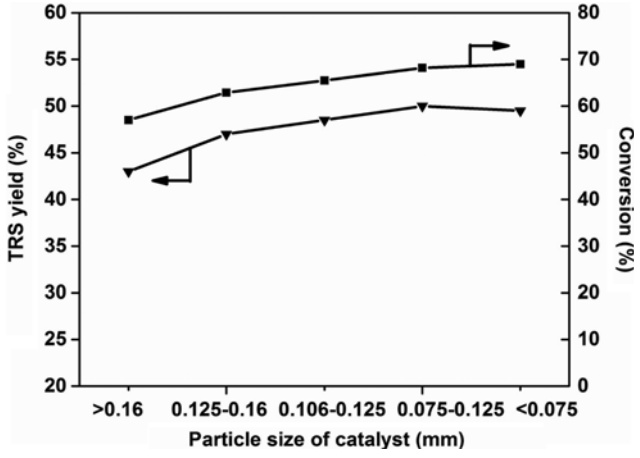

Fig. 8. Effect of particle size of catalyst on the hydrolysis of MCC (180 °C reaction temperature, 3 of time, 6 mg/mL concentration, mass ratio 3.3 : 1).

(w/w). When the mass ratio is 3.3, the catalyst can provide enough active sites for the conversion of MCC and increases the opportunity of solid-solid contact between MCC and catalyst, which would be beneficial to the hydrolysis of MCC.

2-3. Effect of Particle Size of Catalyst on the Hydrolysis of MCC

The effect of particle size of catalyst on the hydrolysis of MCC is shown in Fig. 8. There is no noticeable difference in catalytic activity among these catalyst samples, suggesting that the reaction is not influenced obviously by the particle size in the range of 0.075-1.6 mm. The particle size of catalyst used in this experiment is smaller than 0.075 mm.

2-4. Reaction Kinetic Analysis

Generally, the rate controlling step of diffusion of cellulose to solid is much more difficult than hydrolysis reaction, which occurs in the surface and pore channels [39,40]. On one hand, the effect of particle size of catalyst on the hydrolysis of MCC is no noticeable difference in the range of 0.075-1.6 mm shown in Fig. 8. On the other hand, the adsorption capability of carboxyl groups in catalyst for cellulose can eliminate the problem of mass-transfer limitation in a very good way and increase the solid-solid contact opportunity significantly, finally leading to an obvious decrease in the activation energy required for the hydrolysis of cellulose and an increase in the formation rate of reducing sugars [41]. Thus, the kinetic equation developed is based on the chemical reaction step.

According to previous empirical formulas [34,42,43], the MCC hydrolysis reaction follows the pseudo-first-order, which includes two consecutive reactions:

$$\text{Cellulose (C)} \xrightarrow{k_1} \text{Reducing sugar (R)} \qquad (3)$$
$$\xrightarrow{k_2} \text{Degradation products (D)}$$

In accordance with Eq. (3), the reducing sugar producing rate is:

$$\frac{dC_R}{dt} = k_1 C_C - k_2 C_R \qquad (4)$$

which, integrated, lead to:

$$C_R = C_{Co}\frac{k_1}{k_1 - k_2}[e^{-k_1 t} - e^{-k_2 t}] \qquad (5)$$

the cellulose hydrolysis rate constant is as follows:

$$\frac{dC}{dt} = -k_C C_C \qquad (6)$$

which, integrated, leads to:

$$\ln\left(\frac{C_C}{C_{Co}}\right) = -\ln(1-X) = k_C t \qquad (7)$$

where k_c is the pseudo-first-order of cellulose hydrolysis rate constant (h^{-1}); k_1 is the reducing sugar producing rate constant (h^{-1}); k_2 is the reducing sugar degradation rate constant (h^{-1}); X is the conversion of MCC.

The plot of $-\ln(1-X)$ as a function of reaction time shows good linearity in 1-6 h at different temperature, and the result is shown in Fig. 9(a). The reaction rate constant k follows Arrhenius equation (Eq. (8)), and the further transformation is shown as Eq. (9).

Table 4. The kinetic parameters for MCC hydrolysis

T/K	k_c/h^{-1}	R^2
423	0.124	0.951
433	0.194	0.987
443	0.247	0.990
453	0.262	0.988
$k_C=3.1\times10^{11}$ exp (−137.18/RT)		0.997

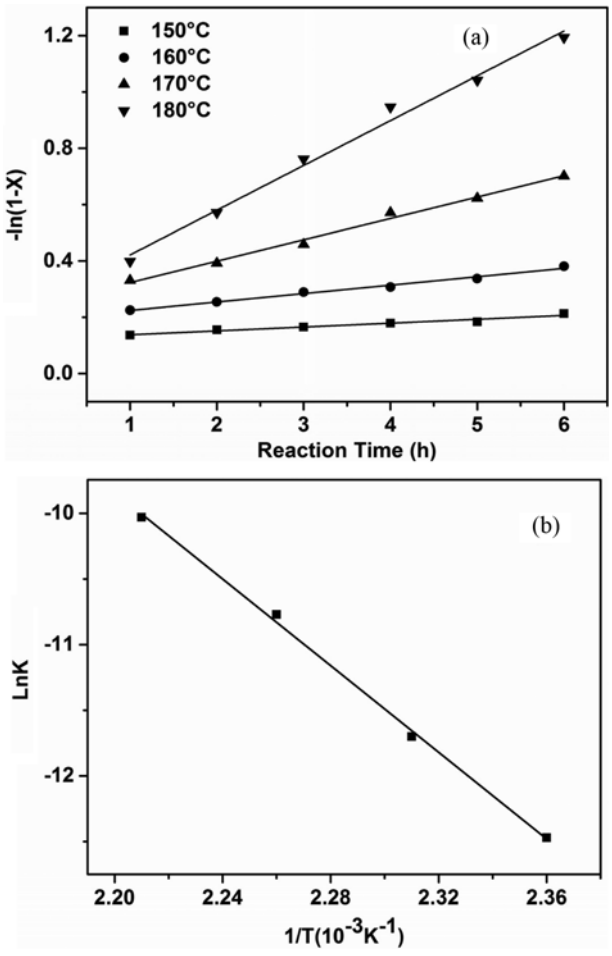

Fig. 9. Cellulose hydrolysis rate constant (a) and Arrhenius plot (b) of hydrolysis reactions of MCC on LPC-SO_3H.

$$k = Ae^{\left(-\frac{E_a}{RT}\right)} \quad (8)$$

$$\ln k = -\frac{E_a}{RT} + \ln A \quad (9)$$

where A is the pre-exponential factor (h^{-1}); E_a is the activation energy (kJ/mol).

The activation energy (E_a) of MCC hydrolysis is 137.18 kJ/mol at 423-453 K as shown in Fig. 9(b), and the pre-exponential factor is 3.1×10^{11} h^{-1}.

According to the data of TRS yield at different temperatures, the kinetic parameters for TRS production and degradation are evaluated using the non-linear least squares in Matlab 7.0. The TRS producing rate constant k_1 and its degradation rate constant k_2 are calculated and listed in Table 5. As can be seen, k, k_1 and k_2 all increase with the increase of reaction temperature. When reaction temperature is greater than 453 K, k_1 is greater than k_2, which suggests that the temperature higher than 453 K is beneficial to the formation of reducing sugar.

Table 5. The kinetic parameters for TRS production and degradation

T/K	k_1/h^{-1}	k_2/h^{-1}	R^2
423	0.081	0.150	0.994
433	0.130	0.186	0.982
443	0.206	0.252	0.994
453	0.394	0.364	0.990
463	0.571	0.453	0.979
$k_1=1.5\times10^9$ exp (−83.306/RT)			0.993
$k_2=1.2\times10^5$ exp (−48.055/RT)			0.990

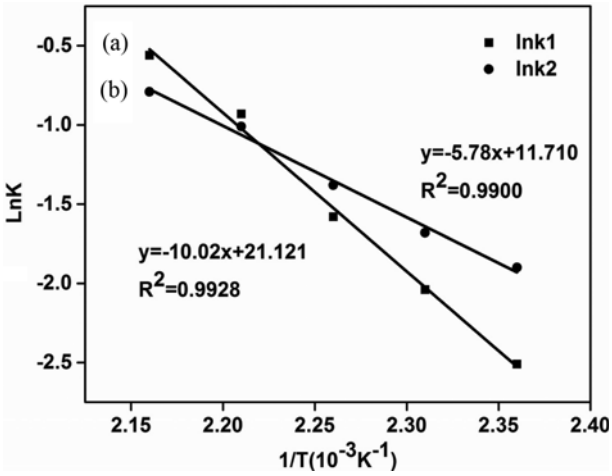

Fig. 10. Arrhenius plot of hydrolysis reactions of TRS production (a) and degradation (b).

Through the linear fitting between lnk and 1/T depicted in Fig. 10, the pre exponential factor of TRS production and degradation of 1.5×10^9 h^{-1} and 1.5×10^5 h^{-1} are obtained, and the reaction activation energy is 83.31 kJ/mol and 48.06 kJ/mol at 423-463 K, respectively. The E_a of the MCC hydrolysis by LPC-SO_3H catalyzed reactions is smaller than that by sulfuric acid (170 kJ/mol for MCC) according to the report [34].

CONCLUSIONS

Lignin-derived solid acid catalyst was prepared by carbonization of alkali lignin from pulping industry followed by sulfonation, and the effect of pretreatment for alkali lignin on the catalytic activity of LDSA in MCC hydrolysis was investigated. Results showed that LPC-SO_3H had higher catalytic activity than LC-SO_3H and SLC-SO_3H. It was suggested that the structure of LPC-SO_3H containing higher densities of -COOH group (1.68 mmol/g) as binding site and -SO_3H group (0.88 mmol/g) as catalytic site as well as larger specific surface area of 488.4 m^2/g was mainly responsible

for its better catalytic performance in MCC hydrolysis. In addition, the reaction conditions for MCC hydrolysis were optimized, and the maximum TRS yield of 50.8% was achieved when reaction temperature and time were 180 °C and 3 h, MCC concentration was 6 mg/mL, and mass ratio of catalyst to MCC was 3.3 (w/w). Reaction kinetic analysis demonstrated that LPC-SO_3H could promote the hydrolysis of MCC in water through reducing the activation energy required for hydrolysis. This strategy can prepare a solid acid catalyst with favorable property, which will have a good application in the hydrolysis of cellulose.

ACKNOWLEDGEMENTS

The authors are grateful for the financial support from the Natural Science Foundation of Fujian Province, China (2015J01055), the Scientific Research Allowance of Huaqiao University of China (13BS417) and the Research Innovation Project of Graduate Students in Huaqiao University (2014).

REFERENCES

1. J. Wang, J. Xi and Y. Wang, *Green Chem.*, **17**, 737 (2015).
2. L. Hu, L. Lin, Z. Wu, S. Y. Zhou and S. J. Liu, *Appl. Catal. B: Environ.*, **174**, 225 (2015).
3. L. Hu, X. Tang, Z. Wu, L. Lin, J. Xu and N. Xu, *Chem. Eng. J.*, **263**, 299 (2015).
4. M. Wu, Y. Wang, D. Wang, M. Tan, P. Li, W. Wu and N. Tsubaki, *J. Porous Mater.*, **23**, 263 (2015).
5. Y. Wang, D. Wang, M. Tan, B. Jiang, J. Zheng, N. Tsubaki and M. Wu, *ACS Appl. Mater Interfaces*, **7**, 26767 (2015).
6. L. Zhou, Z. Liu, Y. Bai, T. Lu, X. Yang and J. Xu, *J. Energy Chem.*, **25**, 141 (2016).
7. Y. Zhou, R. Huang, F. Ding, A. D. Brittain, J. Liu, M. Zhang, M. Xiao, Y. Meng and L. Sun, *ACS Appl. Mater Interfaces*, **6**, 7417 (2014).
8. M. X. Cheng, T. Shi, H. Y. Guan, S. T. Wang, X. H. Wang and Z. J. Jiang, *Appl. Catal. B: Environ.*, **107**, 104 (2011).
9. J. Hegner, K. C. Pereira, B. DeBoef and B. L. Lucht, *Tetrahedron Lett.*, **51**, 2356 (2010).
10. R. Rinaldi, R. Palkovits and F. Schuth, *Angew. Chem. Int. Ed.*, **47**, 8047 (2008).
11. Z. W. Fu, H. Wan, Q. Cui, J. H. Xie, Y. J. Tang and G. F. Guan, *React. Kinet. Mech. Cat.*, **104**, 313 (2011).
12. Z. W. Fu, H. Wan, X. S. Hu, Q. Cui and G. F. Guan, *React. Kinet. Mech. Catal.*, **107**, 203 (2012).
13. S. G. Shen, C. Y. Wang, B. Cai, H. M. Li, Y. Han, T. Wang and H. F. Qin, *Fuel*, **113**, 644 (2013).
14. S. G. Shen, B. Cai, C. Y. Wang, H. M. Li, G. Dai and H. F. Qin, *Appl. Catal. A: Gen.*, **473**, 70 (2014).
15. F. Guo, Z. L. Xiu and Z. X. Liang, *Appl. Energy*, **98**, 47 (2012).
16. Y. Y. Wu, Z. H. Fu, D. L. Yin, Q. Xu, F. L. Liu, C. L. Lu and L. Q. Mao, *Green. Chem.*, **12**, 696 (2010).
17. S. Suganuma, K. Nakajima, M. Kitano, D. Yamaguchi, H. Kato, S. Hayashi and M. Hara, *J. Am. Chem. Soc.*, **130**, 12787 (2008).
18. C. G. Zhong, Q. Cao, L. C. Guo and S. B. Deng, *React. Kinet. Mech. Catal.*, **112**, 361 (2014).
19. H. X. Guo, X. H. Qi, L. Y. Li and R. L. Smith, *Bioresour. Technol.*, **116**, 355 (2012).
20. H. X. Guo, Y. F. Lian, L. I. Yan, H. X. Qi and R. L. Smith, *Green Chem.*, **15**, 2167 (2013).
21. X. H. Qi, H. X. Guo, L. Y. Li and R. L. Smith, *Chemsuschem*, **5**, 2215 (2012).
22. M. Ayyachamy, F. E. Cliffe, J. M. Coyne, J. Collier and M. G. Tuohy, *Biomass. Conv. Bioref.*, **3**, 255 (2013).
23. F. L. Pua, Z. Fang, S. Zakaria, F. Guo and C. H. Chia, *Biotechnol. Biofuels*, **4**, 56 (2011).
24. S. Hu and Y. L. Hsieh, *J. Mater. Chem. A*, **1**, 11279 (2013).
25. L. H. Gan, M. S. Zhou and X. Q. Qiu, *Holzforschung*, **69**, 25 (2015).
26. L. H. Gan, M. S. Zhou, D. J. Yang and X. Q. Qiu, *J. Disper. Sci. Technol.*, **34**, 644 (2012).
27. L. Hu, Z. Wu, J. X. Xu, S. Y. Zhou and G. D. Tang, *Korean J. Chem. Eng.*, **1**, 1 (2016).
28. S. X. Hu, F. Jiang and Y. L. Hsieh, *ACS Sustainable Chem. Eng.*, **3**, 2566 (2015).
29. X. C. Zhang, Z. Zhang, F. Wang, Y. H. Wang, Q. Song and J. Xu, *J. Mol. Catal. A: Chem.*, **377**, 102 (2013).
30. G. F. Lin, J. C. Jiang, K. J. Wu and K. Sun, *Bioenergy Res.*, **6**, 1237 (2013).
31. S. Zuo, J. Yang, J. Liu and X. Cai, *Fuel Process Technol.*, **90**, 994 (2009).
32. H. Wikberg, T. Ohra-aho, F. Pileidis and M. M. Titirici, *ACS Sustainable Chem. Eng.*, **3**, 2737 (2015).
33. S. G. Shen, C. Y. Wang, B. Cai, H. M. Li, Y. Han, T. Wang and H. F. Qin, *Fuel*, **113**, 644 (2013).
34. L. Shuai and X. J. Pan, *Energy Environ. Sci.*, **5**, 6889 (2012).
35. S. L. Hu, T. J. Smith, W. Y. Lou and M. H. Zong, *J. Agric. Food Chem.*, **62**, 1905 (2014).
36. Y. Xiong, Z. H. Zhang, X. Wang, B. Liu and J. T. Lin, *Chem. Eng. J.*, **235**, 349 (2014).
37. Z. Sun, M. L. Tao, Q. Zhao, H. Y. Guang, T. Shi and X. H. Wang, *Cellulose*, **22**, 675 (2015).
38. A. Onda, T. Ochi and K. Yanagisawa, *Green Chem.*, **10**, 1033 (2008).
39. D. M. Lai, L. Deng, Q. X. Guo and Y. Fu, *Energy Environ. Sci.*, **4**, 3552 (2011).
40. D. M. Lai, L. Deng, J. Li, B. Liao, Q. X. Guo and Y. Fu, *ChemSusChem*, **4**, 55 (2011).
41. J. Wang, J. Ren, X. Liu, G. Lu and Y. Wang, *AIChE J.*, **59**, 2558 (2013).
42. Z. Yang, R. Huang, W. Qi, L. Tong, R. Su and Z. He, *Chem. Eng. J.*, **280**, 90 (2015).
43. H. Kobayashi, Y. Ito, T. Komanoya, Y. Hosaka, P. L. Dhepe, K. Kasai, K. Hara, A. Fukuoka, *Green Chem.*, **13**, 326 (2011).